Relativistic effects on spin observables in quasielastic proton scattering

C. J. Horowitz
Laboratory for Nuclear Science and Department of Physics, Center for Theoretical Physics, Massachusetts Institute of Technology, Cambridge, Massachusetts 02139

M. J. Iqbal
TRIUMF, Vancouver, British Columbia, Canada
(Received 9 December 1985)

The spin observables in quasielastic proton scattering are calculated in a simple relativistic model where the NN interaction is assumed to depend on the enhancement of the lower components of nucleon wave functions (because of strong nuclear potentials). This enhancement is characterized by an average effective mass M^* of $(0.8-0.9)M$ which is calculated in an eikonal model. The M^* dependence of the NN interaction is taken from relativistic impulse approximation calculations. The polarization is found to decrease by 40 percent compared to the free NN value at 500 MeV. Next, simple formulas are provided to estimate the effects of spin-orbit potential distortions on spin observables. At 500 MeV and 18.5° in ^{208}Pb, the polarization is decreased by 5 percent while $D_{l'l}$ and $D_{s's}$ are decreased by 15 percent and D_{nn} is almost unchanged.

I. INTRODUCTION

Most of the relativistic approaches to nuclear physics suggest that the optical potential or self-energy for a nucleon in the nucleus involves large attractive Lorentz scalar and repulsive vector contributions. Relativistic mean field calculations[1] relate these potentials to large sigma (scalar) and omega (vector) meson fields and provide a good description of ground state charge densities. Dirac optical model fits to elastic proton scattering[2] also use strong potentials to reproduce analyzing power data. Finally, relativistic impulse approximation (RIA) calculations[3] find strong potentials coming from large scalar and vector pieces of a Lorentz invariant representation of the NN amplitudes. These RIA calculations provide an excellent description of elastic scattering at 500 MeV and above.

However, most of these scattering calculations have involved relativistic effects on the projectile in an elastic scattering. One would like to look for characteristic signatures of the strong potentials as seen through inelastic reactions. In this paper, we examine spin observables in quasielastic proton scattering. We consider quasielastic scattering to the continuum in order to minimize the uncertainties in the nuclear structure of discrete final states. Quasielastic scattering is modeled in a distorted wave impulse approximation (DWIA). Here, a single hard scattering, described by the NN interaction in the medium, takes place between distorted incoming and outgoing waves (treated in an eikonal approximation).

There have been some relativistic calculations for quasielastic *electron* scattering, for example, Refs. 10, 20 and 21. However, for electrons there are no spin observables with clear relativistic signatures. To our knowledge, no previous relativistic calculations for quasielastic proton scattering have been done.

To minimize corrections from multiple hard scattering (where two or more nucleons are knocked out) and distortion effects, we look near the maximum in the quasielastic peak (energy transfer near $q^2/2M$). In addition, we look at spin observables rather than cross sections since the latter are greatly reduced by the distortions. In contrast, the spin dependence of the distortions is not expected to be strong (although we examine the effect of the spin-orbit optical potential in Sec. III). The NN interaction in the medium could differ from the free interaction for a number of reasons. First, Pauli blocking and binding energy corrections should be incorporated. However, these corrections are not expected to be large at the relatively low densities (about $\frac{1}{4}$ to $\frac{1}{3}$ of nuclear matter density) of surfaced peaked quasifree scattering.

In a relativistic approach the NN interaction depends on the four-component Dirac wave functions. The lower components of these wave functions are enhanced in the medium due to strong potentials. This enhancement is characterized by an effective mass M^* which is smaller than the free mass M of a nucleon. The lower components for a nucleon of momentum p are now of order p/M^* which is increased from the free value of p/M. If one thinks of the NN interaction $\hat{F}$ as a 4×4 matrix in the spinor space of the two nucleons, then the NN amplitudes K will change as one changes the Dirac spinors U used to take matrix elements of $\hat{F}$.

$$K(M^*)=2ik_c\bar{U}(1',M^*)\bar{U}(2',M^*)\hat{F}U(1,M^*)U(2,M^*)\ . \tag{1}$$

Here, 1 (1′) describes the spin and momentum of the incoming (outgoing) first particle and k_c is the momentum in the two-body center of mass frame.

If single scattering dominates the reaction mechanism then the spin observables in quasielastic scattering will simply be equal to those calculated from the amplitudes K

evaluated at some average M^* (see Sec. II). These spin observables may be sensitive to even small changes in M^* since the RIA uses a representation for $\hat{F}$ which involves sensitive cancellations between strong Lorentz scalar and vector contributions. As M^* decreases the importance of the vector repulsion will grow with respect to the scalar attraction.

In the original RIA (Ref. 3) free spinor matrix elements of Eq. (1) with $M^*=M$ where equated to the experimental NN amplitudes to obtain the five functions F_i in the following *model* for $\hat{F}$.

$$\hat{F}=\sum_{i=s}^{t} F_i(E,q)\lambda_i^1\cdot\lambda_i^2 . \tag{2a}$$

Here, λ_i^1 are a set of Dirac matrices for the first particle and the dot signifies contraction over all Lorentz indices. The Lorentz invariant amplitudes F_i are functions of energy E and momentum transfer q. The set of Dirac matrices used in this model is

i	λ_i
s (scalar)	1
v (vector)	γ^μ
p (pseudoscalar)	γ_5
a (axial vector)	$\gamma_5\gamma^\mu$
t (tensor)	$\sigma^{\mu\nu}$

(2b)

Since all that the two-nucleon data determines is the matrix element of Eq. (1) with $M^*=M$, there must be a model dependence in Eq. (2) for M^* not equal to M. In general, there are an infinite number of operators $\hat{F}$ with identical matrix elements for $M^*=M$ but different ones for $M^*\neq M$. The special form adopted in Eq. (2) assumes that the NN interaction (in the Dirac representation) is reasonably local, i.e., there are no factors of momentum dotted into a gamma matrix in Eq. (2). This appears to be a good approximation at energies of 500 MeV and above where the original RIA [which assumes Eq. (2)] works very well.[4] In the future *one may be able to use the spin observables in quasielastic proton scattering to examine experimentally the form of* $\hat{F}$ and see if Eq. (2) is a good approximation.

In Sec. II we describe our eikonal model for the projectile wave function and use it to calculate the average density, effective mass, and impact parameters appropriate for each nucleus and energy. We consider incident laboratory kinetic energies of 200, 400, 500, 800, and 1000 MeV. In Sec. III, we calculate how the spin observables depend on M^*. Next, Sec. IV examines the effect of the distortions from the spin-orbit optical potentials on spin observables. We sum up results in Sec. V and discuss further applications of the model in Sec. VI. Nuclei considered are ^{12}C, ^{40}Ca, ^{90}Zr, and ^{208}Pb.

II. EIKONAL FORMALISM

An eikonal approximation to the incoming (+) or outgoing (−) distorted wave of the projectile in scalar S and vector V optical potentials is[5]

$$\psi_{ks}^{\pm}=\left[\frac{E+M}{2M}\right]^{1/2}\begin{bmatrix}1\\ \dfrac{\sigma\cdot\mathbf{p}}{E+M+S-V}\end{bmatrix}e^{i\mathbf{k}\cdot\mathbf{x}}e^{iS^{\pm}(x)}\chi_s , \tag{3}$$

where k is the projectile momentum, χ_s a Pauli spinor, and the phase factor $S(z)$ is

$$S^{\pm}(z)=-\int_{\mp\infty}^{z}\frac{M}{k}dz'[V_c(b,z') + V_{so}(b,z')(\sigma\cdot\mathbf{b}\times\mathbf{k}-ikz')] . \tag{4}$$

Here the effective central V_c and spin-orbit V_{so} potentials are

$$V_c=S+\frac{E}{M}V+\frac{1}{2M}(S^2-V^2) , \tag{5}$$

$$V_{so}=-\frac{1}{2Mr}\frac{\frac{\partial}{\partial r}(S-V)}{E+M+S-V} . \tag{6}$$

We shall omit V_{so} as a first approximation (and consider its effects in Sec. III).

The transmission probability for going through the nucleus at an impact parameter b is

$$T(b)=|e^{iS^{+}(\infty)}|^2=\exp\left[\frac{4M}{k}\int_0^\infty dz\,\mathrm{Im}V_c\right] . \tag{7}$$

We chose to define an average density for given impact parameter as

$$\bar{\rho}(b)=\frac{\int_0^\infty dz\{\rho[(b^2+z^2)^{1/2}]\}^2}{\int_0^\infty dz\,\rho[(b^2+z^2)^{1/2}]} . \tag{8}$$

Then the average density for forward angle scattering from the nucleus is

$$\langle\bar{\rho}\rangle\equiv\frac{\int_0^\infty b\,dbT(b)\bar{\rho}(b)^2}{\int_0^\infty b\,dbT(b)\bar{\rho}(b)} . \tag{9}$$

Clearly, this expression weighs more trajectories with large impact parameters where $T(b)$ is near one. Therefore, the reaction is surfaced peaked and $\langle\bar{\rho}\rangle$ is less than half normal density. For quasielastic electron scattering we define an average density by setting $T(b)=1$ in Eq. (9). This leads to significantly higher values of $\langle\bar{\rho}\rangle$.

Given an average density for the reaction, one can estimate an average scalar field strength S and from S calculate an effective mass. We assume the scalar field is proportional to the density and use

$$\begin{aligned} M^*&=M+S ,\\ \langle M^*\rangle/M&=1.0-0.44\langle\bar{\rho}\rangle , \end{aligned} \tag{10}$$

where $\langle\bar{\rho}\rangle$ is measured in units of the nuclear matter saturation density and the 0.44 results from the mean field theory[6] which gives

$$M^*/M=0.56 \tag{11}$$

at nuclear matter saturation density.

Table I gives average densities and effective masses for various nuclei. Here Wood-Saxon optical parameters are

TABLE I. Average density effective masses $\langle M^* \rangle$ and impact parameters $\langle b \rangle$ for various nuclei. The average density $\langle \bar{\rho} \rangle$ is given by Eq. (9) while $\langle M^* \rangle$ is from Eq. (10) and $\langle b \rangle$ from Eq. (47). The electron scattering $\langle M^* \rangle_{ee'}$ is from Eq. (9) with $T(b)=1$. The optical potentials used are from Ref. 7 (for ^{12}C, ^{40}Ca potentials were used with R scaled by $A^{1/3}$), while the densities used are in Table II.

	T_{lab} (MeV)	$\langle \bar{\rho} \rangle$ ρ_0	$\langle M^* \rangle$ M	$\langle M^* \rangle_{ee'}$ M	Optical Potential see Ref. 7	$\langle b \rangle$ (fm)
^{12}C	200	0.36	0.84	0.80	(^{40}Ca)4	2.14
	400	0.37	0.84		7	2.12
	500	0.29	0.87		9	2.41
	800	0.23	0.90		12	2.66
^{40}Ca	200	0.42	0.81	0.74	4	3.38
	400	0.43	0.81		7	3.33
	500	0.32	0.86		9	3.82
	800	0.28	0.89		12	4.14
^{90}Zr	160	0.42	0.82	0.70	1	4.76
	500	0.27	0.88		2	5.40
	800	0.30	0.87		4	5.24
^{208}Pb	200	0.38	0.83	0.68	3	6.66
	400	0.35	0.85		5	6.80
	500	0.31	0.86		7	6.95
	800	0.25	0.89			

taken from Ref. 7 and crude Wood-Saxon fits to the relativistic Hartree densities of Ref. 1 are used. These densities are given in Table II. The average density varies from 0.25 to 0.4. The density is higher at the lower energies where the nucleus is more transparent. It is important to emphasize that there is very little A dependence. The average density is almost the same in ^{12}C, ^{40}Ca, and ^{208}Pb because the reaction is surfaced peaked, i.e., $T(b)$ is very small for trajectories which pass near the center of Pb.

Therefore, if one is looking for medium effects, going to a heavy nucleus does not gain one anything. In fact, a heavy nucleus will have larger spin-orbit distortions (see Sec. III) and presumably more background from multiple scatterings. Thus, it may be simpler to interpret spin observables in light nuclei.

We now calculate the position of the quasielastic peak. The single particle spectrum $E(k)$ as a function of momentum k is given by

TABLE II. Baryon density parameters (crudely) fitted to the relativistic Hartree calculations of Ref. 1, $\rho(r)/\rho_0=[1+\exp(r-R)/a]^{-1}$.

Nucleus	R (fm)	a (fm)
^{12}C	2.08	0.477
^{40}Ca	3.57	0.514
^{90}Zr	4.96	0.486
^{208}Pb	6.69	0.530

$$E(k)=\langle V \rangle+(k^2+\langle M^* \rangle^2)^{1/2} . \quad (12)$$

This is for nuclear matter with an average vector potential $\langle V \rangle$ at an effective mass $\langle M^* \rangle$. The maximum in the quasielastic peak (for a momentum transfer q) occurs at an energy loss $E(q)-E(0)$. If we assume $\langle V \rangle$ and $\langle M^* \rangle$ to be independent of k then the energy loss is independent of $\langle V \rangle$.

$$E(q)-E(0)=(q^2+\langle M^* \rangle^2)^{1/2}-\langle M^* \rangle . \quad (13)$$

This energy loss is increased from that for free scattering off of a mass M. This gives a "binding energy shift" of

$$\Delta E=(q^2+\langle M^* \rangle^2)^{1/2}-(q^2+M^2)^{1/2}-\langle M^* \rangle+M . \quad (14)$$

However, this binding energy shift is substantially smaller than that for electron scattering because $\langle M^* \rangle$ is much larger for the surfaced peaked proton reaction. The position of the quasielastic peak in ^{12}C at 1000 MeV is shown in Fig. 1 using Eq. (13) and the 800 MeV $\langle M^* \rangle$ value from Table I. The agreement with experiment[8] is very good. If instead the lower electron scattering value of $\langle M^* \rangle$ is used the binding energy shift is too large. A nonrelativistic shell model with typical binding energies for the s and p states will also substantially overestimate the binding energy shift.[9]

Note that this description of the binding energy shift is oversimplified. For heavier nuclei, one needs to consider Coulomb corrections. Since the Coulomb potential slows the projectile down, it will transfer less momentum to the struck nucleon and the binding energy shift will be significantly reduced. This effect could be 5 MeV or more in Pb and thus eliminate much of the shift due to M^*, leaving a

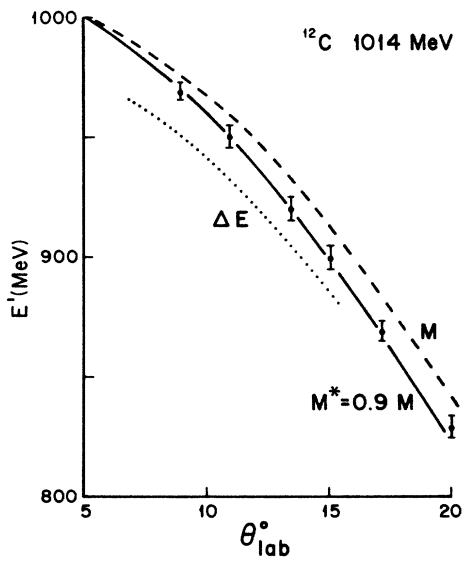

FIG. 1. Position of the quasielastic peak (energy of scattered proton) versus laboratory scattering angle for 1014 MeV scattering from ^{12}C. The dashed curve is for free NN scattering while the solid curve is Eq. (3) for an $\langle M^* \rangle$ of $0.89M$. Finally the dotted curve is shifted from the dashed curve by $\Delta E = 25$ MeV which is the much larger binding energy shift found in electron scattering (Ref. 10). The experimental data is from Ref. 8.

peak near the free NN position. One should also consider the nuclear potential. However, in relativistic models the "wine bottle bottom" shape of V_c is crossing zero in the surface regions of interest. Therefore, the average nuclear potential may be small (see Table III).

It remains to examine the effects of multiple hard scattering on the position of the peak. These could be sizable since multiple scattering greatly increases the width of the peak in heavy nuclei at large scattering angles. In a latter publication we will consider the position of the quasielastic peak in more detail.

For electron scattering, Rosenfelder[10] found that a value of $\langle M^* \rangle = 0.71M$ provided a good description of 500 MeV quasielastic electron scattering from ^{40}Ca. His value is very close to our value of $0.74M$ predicted by Eqs. (9) and (10) with $T(b) = 1.0$. Thus, our simple model of $\langle M^* \rangle$ provides a good description of the binding energy shifts in electron scattering.

III. EFFECTIVE MASS DEPENDENCE OF NN OBSERVABLES

We now calculate the M^* dependent observables implied by Eq. (1). One representation of the NN amplitude $K(\langle M^* \rangle)$ is[11]

$$K(\langle M^* \rangle) = \tfrac{1}{2}[a + b + (a-b)\sigma_{1n}\sigma_{2n} + (c+d)\sigma_{1m}\sigma_{2m} + (c-d)\sigma_{1l}\sigma_{2l} + e(\sigma_{1n} + \sigma_{2n})] \ . \quad (15)$$

Equating this to the positive energy spinor U [of mass $\langle M^* \rangle$, $E^* = (k^2 + \langle M^* \rangle^2)^{1/2}$],

TABLE III. Spin rotation angles [R in Eq. (29)] and real and imaginary central potentials, Eq. (5), evaluated at the average impact parameters $\langle b \rangle$, Eq. (47), in Table I. Densities and optical potentials are as per Table I.

	T_{lab} (MeV)	R	V_{eff} (MeV)	W_{eff} (MeV)
^{12}C	200	$0.175-0.053i$	−30	−14
	400	$0.147-0.036i$	−13	−20
	500	$0.098-0.033i$	0.5	−31
	800	$0.067-0.021i$	0.7	−44
^{40}Ca	200	$0.218-0.067i$	−26	−15
	400	$0.189-0.045i$	−12	−22
	500	$0.110-0.037i$	−1	−26
	800	$0.064-0.018i$	1.3	−31
^{90}Zr	160	$0.244-0.146i$	−26	−14
	500	$0.130-0.081i$	−5	−20
	800	$0.070-0.049i$	2	−36
^{208}Pb	200	$0.253-0.103i$	−21	−15
	400	$0.183-0.062i$	−8	−20
	500	$0.134-0.044i$	−3	−21

$$U(\langle M^* \rangle) = \left[\frac{E^* + \langle M^* \rangle}{2\langle M^* \rangle}\right]^{1/2} \begin{bmatrix} 1 \\ \dfrac{\boldsymbol{\sigma}\cdot\mathbf{k}}{E^* + \langle M^* \rangle} \end{bmatrix} \chi_s \ , \quad (16)$$

matrix elements of $\hat{F}$ [Eqs. (1) and (2)], one can derive a 5×5 matrix relating the $a, \ldots, e$ to the five F_i. Note, E^* is just a parameter, the energy is given by Eq. (12). (This matrix is easy to derive by using a helicity basis as an intermediate step, see also Ref. 12.)

$$\begin{bmatrix} a \\ b \\ c \\ d \\ e \end{bmatrix} = \begin{bmatrix} M(k_c, \langle M^* \rangle) \\ \text{see} \\ \text{Appendix A} \end{bmatrix} \begin{bmatrix} F_s \\ F_v \\ F_p \\ F_a \\ F_t \end{bmatrix} . \quad (17)$$

This matrix is a function of the center of mass momentum k_c and the center of mass scattering angle $\theta_{c.m.}$. It also depends on the nucleon's mass as a parameter. If Eq. (2) is a good model for $\hat{F}$ in the medium then one can examine the effects of changes in the wave functions $U(\langle M^* \rangle)$ by simply evaluating Eq. (17) at $\langle M^* \rangle$ not equal to M. Therefore, we will consider Eq. (17) to also be a function of $\langle M^* \rangle$.

The procedures involve two steps. First, $a, \ldots, e$ amplitudes from the Arndt phase shifts[13] are used with the inverse of Eq. (17) in free space with $\langle M^* \rangle = M$ to calculate Lorentz invariants F_i. The F_i are then assumed unchanged in the medium. Next, Eq. (17) is used in the medium at $\langle M^* \rangle$ to calculate new $a, \ldots, e$. These differ from the Arndt phase shift values because the spinors $U(\langle M^* \rangle)$ are different.

It is now a simple matter to calculate spin observables

for quasielastic proton scattering (in a plane wave impulse approximation) from the new $a,\ldots,e$. For example, the polarization P is given by

$$P=\mathrm{Re}(a^*e)/(d\sigma/d\Omega) \tag{18}$$

or one of the spin rotation parameters D_{l0m0}

$$D_{l0m0}=\mathrm{Im}(b^*e)/(d\sigma/d\Omega)\ , \tag{19}$$

where the total intensity or cross section is

$$d\sigma/d\Omega=\tfrac{1}{2}(a^*a+b^*b+c^*c+d^*d+e^*e)\ . \tag{20}$$

(See also Appendix B.)

To gain an insight into the M^* dependence of the observables, we evaluate Eq. (17) in the $\theta_{\mathrm{c.m.}}=0$ limit. The differential "cross section" for forward scattering is

$$d\sigma/d\Omega(\theta=0)=4k_c^2(\,|F_s+\lambda F_v|^2+|2F_t-\lambda F_a|^2 +2|2\lambda F_t-F_a|^2)\ , \tag{21}$$

where the kinematic factor

$$\lambda=1+2k_c^2/\langle M^*\rangle^2 \tag{22}$$

grows with decreasing $\langle M^*\rangle$.

The cross section in Eq. (21) involves a sensitive cancellation between large attractive scalar F_s and repulsive vector F_v amplitudes. As M^* decreases, the contribution from F_s is Lorentz contracted with respect to F_v. Therefore, the cross section will rise dramatically with decreasing M^* and this rise may "dilute" some of the spin observables. However, the "in medium" NN cross section may not be directly observable since the total quasielastic scattering is dominated by distortion effects.

This Lorentz contraction of the F_s contributions compared to F_v is important in many theoretical models. A number of relativistic mean field[1,6] and Brueckner[14] calculations all find that this change with M^* makes the interaction substantially more repulsive in the medium. As a result, relativistic calculations find nuclear matter saturates at a lower density and binding energy than in similar nonrelativistic calculations. It would be extremely useful to have experimental information on this (possible) change of the NN interaction in the medium.

The slope of the polarization with respect to q at forward angles is given by (P itself vanishes at $\theta=0$)

$$dP/dq\,|_{q=0}=-\frac{8k_c^3E_c^*}{\langle M^*\rangle^3}\frac{\mathrm{Im}(F_v^*+2F_t^*)(F_s+F_v+2F_t-F_a)}{\partial\sigma/\partial\Omega(\theta=0)}\ . \tag{23}$$

Here, there are two competing effects as M^* decreases. First, the leading factor grows like $1/2M^{*2}$. However, near $E=800$ MeV the cross section in Eq. (21) grows even faster (because of the sensitive cancellations between F_s and F_v). Therefore, near 800 MeV, P decreases with M^*. Below 400 MeV the two effects nearly cancel and P will be insensitive to M^*.

The spin rotation parameter D_{l0m0} also vanishes at $\theta=0$ and its slope is given by

$$dD_{l0m0}/dq\,|_{q=0}=-\frac{4k_c}{d\sigma/d\Omega}\left\{|F_s+\lambda F_v+F_a-2\lambda F_t|^2+\mathrm{Re}(F_s^*+\lambda F_v^*+F_a^*-2\lambda F_t^*)\times\left[4\lambda F_t-2F_a-\frac{E_c^*}{\langle M^*\rangle}(F_s+F_v+2F_t-F_a)\right]\right\}\ . \tag{24}$$

This Eq. (24) involves cancellations between two terms. At low energies 200–400 MeV and forward angles D_{l0m0} is very sensitive to M^*. It grows substantially more negative as M^* decreases. This is the same energy and angular region where the spin rotation parameter Q in N-nucleus elastic scattering changes rapidly with energy. At higher energies D_{l0m0} is insensitive to M^*.

IV. SPIN-ORBIT DISTORTIONS

Before comparing the calculations in Sec. III to data, we examine the effects of spin dependent distortions on the spin observables in quasielastic scattering. This discussion is completely general and applies to any relativistic or nonrelativistic description independent of our model for M^*.

In a distorted wave impulse approximation, the transition amplitude for the projectile scattering from $|i\rangle$ to $|f\rangle$ is

$$M_{fi}=\langle f\,|\,K_{\mathrm{lab}}\,|\,i\rangle\ . \tag{25}$$

Here K_{lab} is the NN amplitude in the laboratory frame and $|i\rangle$ is an incoming distorted wave. In this section we will only be interested in the spin dependence of $|i\rangle$ so we write

$$|i\rangle=\exp[iS_\sigma^+(x)]\ , \tag{26}$$

$$|f\rangle=\exp[-iS_\sigma^-(x)]\ . \tag{27}$$

Here, S_σ^+ (S_σ^-) will be approximately evaluated at $z=0$ and some impact parameter b.

$$S_\sigma^\pm(b)=-\int_{\mp\infty}^{0}\frac{M}{k}dz'V_{\mathrm{so}}\boldsymbol{\sigma}\cdot\mathbf{b}\times\mathbf{k}\ . \tag{28}$$

Note, we neglect the Darwin term [$-ikz'$ in Eq. (4)] in the eikonal wave function. This term does not destroy flux but moves it to regions of lower density. The Darwin

term remains to be investigated but its effect may largely cancel against the density dependence of the cross section, Eq. (21).

The spin-orbit potential rotates the spin through a complex angle R.

$$
\begin{aligned}
&S_\sigma^+ = R(N\hat{n} + S\hat{s})\cdot\sigma \ , \\
&R = -Mb\int_0^\infty dz' V_{so}[(b^2+z'^2)^{1/2}] \ , \\
&N = (\hat{\mathbf{b}}\times\hat{\mathbf{k}})\cdot\hat{\mathbf{n}} \ , \\
&S = (\hat{\mathbf{b}}\times\hat{\mathbf{k}})\cdot\hat{\mathbf{s}} \ , \\
&\hat{\mathbf{n}} = \mathbf{k}\times\mathbf{k}'/|\mathbf{k}\times\mathbf{k}'| \ , \\
&\hat{s} = \hat{n}\times\hat{k} \ .
\end{aligned}
\tag{29}
$$

Here, N is the component of R in the direction normal to the reaction plane (it only depends on the initial angle of $\hat{b}$ with respect to $\hat{n}$). Next, S is the component of R in the "sideways" direction. The final state factor S^- is given by Eq. (29) with R replaced by $-R$ and the direction $\hat{k}$ replaced by the scattered projectile direction $\hat{k}'$. Note, there is no component of R along the beam axis. The coordinate system is shown in Fig. 2(a).

Polarization transfer observables D_{xy} can now be calculated

$$D_{xy} = \tfrac{1}{4}\mathrm{tr}(\sigma_x M_{fi}\sigma_y M_{fi}^\dagger)/I \ . \tag{30}$$

Here, x is the index for the scattered particle and y, the initial particle index, can take on any of four values $0(\sigma_0=1)$, $\hat{n}$, $\hat{s}$ ($\hat{s}'$), and $\hat{k}$ ($\hat{k}'$). The total intensity is given by

$$I = \tfrac{1}{4}\mathrm{tr}(M_{fi}M_{fi}^\dagger) \ . \tag{31}$$

For completeness we have collected in Appendix B expressions for D_{xy} in the laboratory frame in terms of the $a,\ldots,e$ amplitudes.[11] Equation (30) is related to the free expression without spin-orbit distortions by replacing σ_x with the rotated expression

$$\Sigma_x = \exp(-i\mathbf{R}^*\cdot\boldsymbol{\sigma})\sigma_x\exp(i\mathbf{R}\cdot\boldsymbol{\sigma}) \tag{32a}$$

and σ_y is replaced by

$$\Sigma_y' = \exp(i\mathbf{R}\cdot\boldsymbol{\sigma})\sigma_y\exp(-i\mathbf{R}^*\cdot\boldsymbol{\sigma}) \tag{32b}$$

[i.e., Eq. (30) with M_{fi} calculated with distorted waves is equal to a plane wave calculation with $\sigma_x\to\Sigma_x$ and $\sigma_y\to\Sigma_y'$].

We expand to first order in the small angle R and assume that S averaged over the angle between $\hat{b}$ and $\hat{n}$ will give zero.

$$\langle S\rangle = 0 \ . \tag{33}$$

We will consider different path lengths for finite but small scattering angles in order to calculate a nonzero $\langle N\rangle$. There will be an extra path length L for a straight line trajectory of impact parameter b which scatters at

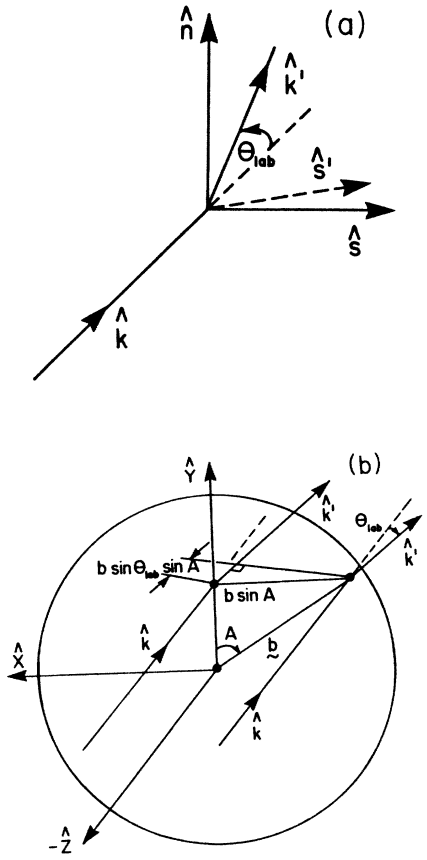

FIG. 2. (a) Incident and scattered projectile coordinate systems. The projectile scatters from $\hat{\mathbf{k}}$ to $\hat{\mathbf{k}}'$ and $\hat{\mathbf{n}}\propto\hat{\mathbf{k}}\times\hat{\mathbf{k}}'$ is the normal to the reaction plane. The incident polarization can be resolved along $\hat{\mathbf{n}},\hat{\mathbf{k}}$ (or l=longitudinal) and $\hat{\mathbf{s}}=\hat{\mathbf{k}}\times\hat{\mathbf{n}}$ (sideways) directions. For the outgoing particle $\hat{\mathbf{s}}'=\hat{\mathbf{k}}'\times\hat{\mathbf{n}}$ is the new sideways direction. (b) Path length differences for scattering from $\hat{\mathbf{k}}$ to $\hat{\mathbf{k}}'$ through an angle $\theta_{\rm lab}$. Here, the initial direction $\hat{\mathbf{k}}$ is parallel to the z axis. The favored trajectory (shorter path length for given b) scatters from the near side of the nucleus (right-hand side or $-\hat{\mathbf{x}}$). The path length is shorter by an amount $b\sin(\theta_{\rm lab})\sin(A)$, Eq. (34), compared to the trajectory with $A=0$.

TABLE IV. Spin observables for 500 MeV p-^{208}Pb scattering at 18.5 (deg) in the laboratory. The free $M^*=M$ numbers are isospin averages of pp and pn observables from Arndt weighted by Z/A and N/A (Ref. 13). Those with $L\cdot S$ use Eqs. (40)–(46) to include spin-orbit distortions.

	$M^*=M$		$M^*=0.86M$	
Observable	Free	with $L\cdot S$	Free	with $L\cdot S$
P	0.41	0.38	0.28	0.25
D_{nn}	0.82	0.82	0.83	0.83
$D_{l'l}$	0.40	0.36	0.52	0.47
$D_{s's}$	0.47	0.43	0.63	0.58
$D_{s'l}$	0.46	0.51	0.50	0.54
$D_{l's}$	−0.49	−0.54	−0.54	−0.60

$z=0$ through an angle $\theta_{\rm lab}$ (compared to the trajectory which goes through $b=0$).

$$L=-b\sin(\theta_{\rm lab})\sin(A)\ . \tag{34}$$

Here A is the angle of $\hat{b}$ with respect to $\hat{n}$ [see Fig. 2(b)]. The different path lengths will contribute relative amounts depending on the phase factor from the central potential e^{iS}

$$|e^{iS}|^2=\exp[-2MbW_{\rm eff}\sin(\theta_{\rm lab})\sin(A)/k]\ , \tag{35}$$

where $W_{\rm eff}$ is the imaginary part of V_c calculated approximately at $z=0$ and impact parameter b [see Eqs. (4) and (5)]. It is now easy to average N over the angle A

$$\langle N\rangle=\int_0^{2\pi}dA\,\sin(A)\exp[-F\sin(A)]\Big/\int_0^{2\pi}dA\,\exp[-F\sin(A)]\ . \tag{36}$$

Here, the parameter F is

$$F=-2Mb\sin(\theta_{\rm lab})W_{\rm eff}/k\ . \tag{37}$$

Equation (36) is a simple integral given by modified bessel functions

$$\langle N\rangle=-I_1(F)/I_0(F)\underset{F\ll 1}{\approx}-F/2\ . \tag{38}$$

This has limits of -1 for strong absorption (large F) and averages to zero just like Eq. (33) as F goes to zero. Equation (38) describes the extent to which near side scattering [Fig. 2(b)] is favored over far side.

The observables to first order in R are now easy to calculate. The normalization is given by

$$I=1-4\langle N\rangle{\rm Im}RP^0\ . \tag{39}$$

Here, P^0 is the polarization in the absence of $L\cdot S$ distortions. This equation shows that the imaginary $L\cdot S$ potential polarizes an initially unpolarized beam by preferentially absorbing different spin states.

The polarization $P=D_{n0}$ is given by

$$P=ZP^0-2\langle N\rangle{\rm Im}R\,(1+D^0_{nn})\ , \tag{40}$$

$$Z=1+4\langle N\rangle{\rm Im}RP^0\ . \tag{41}$$

Here, the superscript zero refers to an undistorted NN observable. When measuring P we see that the imaginary $L\cdot S$ potential may destroy some of the initial polarization (the one in the second term). Alternatively, one can start with a polarized beam and use the imaginary $L\cdot S$ outgoing distortion to analyze the normal polarization to obtain the D^0_{nn} term.

$$D_{nn}=ZD^0_{nn}-4\langle N\rangle{\rm Im}RP^0\ . \tag{42}$$

Here if the imaginary $L\cdot S$ potential destroys either the incoming or outgoing polarization you wind up measuring P^0. Since D_{nn} is often near one the plus term in Z cancels most of the minus term leaving very small distortion corrections to D_{nn}. The other spin observables are given by

$$D_{s's}=ZD^0_{s's}+2\langle N\rangle{\rm Re}R\,(D^0_{s'l}-D^0_{l's})\ , \tag{43}$$

$$D_{l'l}=ZD^0_{l'l}+2\langle N\rangle{\rm Re}R\,(D^0_{s'l}-D^0_{l's})\ , \tag{44}$$

$$D_{l's}=ZD^0_{l's}+2\langle N\rangle{\rm Re}R\,(D^0_{s's}+D^0_{l'l})\ , \tag{45}$$

$$D_{s'l}=ZD^0_{s'l}-2\langle N\rangle{\rm Re}R\,(D^0_{s's}+D^0_{l'l})\ . \tag{46}$$

Here a spin initially in the $\hat{s}$ direction can be rotated about the $\hat{n}$ axis into the $\hat{l}$ direction. These distortions depend on the real part of R which will be bigger than ImR given that the imaginary $L\cdot S$ potential [see Eqs. (29) and (6)] is often smaller than the real potential.

Equations (40)–(46) form the main results of this section. The angle R depends on the $L\cdot S$ optical potential through Eqs. (29) and (6) while $\langle N\rangle$ depends on the laboratory scattering angle and the imaginary part of the central potential $W_{\rm eff}$ through Eqs. (37), (38), and (5). All of these quantities depend on the impact parameter b. To obtain an estimate of spin-orbit effects we will simply use an average impact parameter $\langle b\rangle$ defined in analogy with the average density [see Eq. (9)].

$$\langle b\rangle=\int_0^\infty b\,db\,bT(b)\bar{\rho}(b)\Big/\int_0^\infty b\,db\,T(b)\bar{\rho}(b)\ . \tag{47}$$

We note that $\rho(\langle b\rangle)$ is about $\langle\bar{\rho}\rangle$. As an example, we consider 500 MeV proton scattering from ^{208}Pb at a scattering angle of 18.5 deg in the laboratory. These are

TABLE V. Spin observables (average of pp and pn) at 500 MeV without $L\cdot S$ distortions.

$\theta_{\rm c.m.}$	$\theta_{\rm lab}$	P	D_{nn}	$D_{s's}$	$D_{s'l}$	$D_{l's}$	$D_{l'l}$
			$M^*=M$				
10°	4.5°	0.21	0.73	0.45	0.00	0.01	0.55
30°	13.4°	0.46	0.81	0.43	0.22	−0.22	0.41
50°	22.5°	0.35	0.82	0.50	0.51	−0.54	0.42
			$M^*=0.86M$				
10°	4.5°	0.19	0.79	0.55	0.10	−0.09	0.66
30°	13.4°	0.33	0.80	0.62	0.35	−0.37	0.52
50°	22.5°	0.25	0.82	0.65	0.52	−0.57	0.53

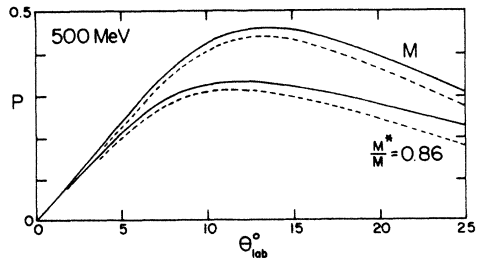

FIG. 3. Polarization (average of pp and pn) versus scattering angle at the quasielastic peak. The solid lines are predictions without $L\cdot S$ distortions while the dotted lines include $L\cdot S$ distortions for ^{208}Pb.

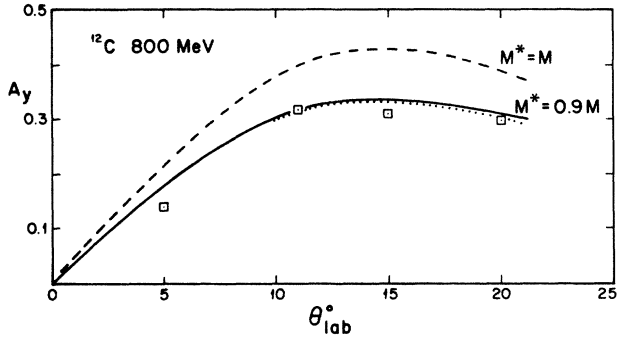

FIG. 4. Analyzing power in ^{12}C at the quasielastic peak at 800 MeV versus laboratory scattering angle. The dashed curve is the free NN prediction (average of pp and pn) while the solid curve is for an M^* of $0.89M$ and the dots include the very small $L\cdot S$ distortion corrections to the solid curve, Eq. (40). The data are from Ref. 19.

the conditions of the Carey *et al.*[15] experiment. Using the Pb density from Table II (and the optical potentials from Ref. 7, case 7) we have

$$\langle b\rangle = 6.95 \text{ fm} . \tag{48}$$

At this impact parameter

$$R = 0.134 - 0.043i , \tag{49}$$

$$\langle N\rangle = -0.20 . \tag{50}$$

These numbers lead to the following changes in observables (see Table IV):

$$P \text{ about 5\% less than } P^0 , \tag{51}$$

$$D_{nn} \text{ almost unchanged} , \tag{52}$$

$$D_{l'l},\ D_{s's} \text{ decrease by about 150004} . \tag{53}$$

If one is interested in the longitudinal S_l or transverse S_t spin flip probabilities[15]

$$S_l = \tfrac{1}{4}[1 - D_{nn} - (D_{l'l} - D_{s's})/\cos(\theta_{\rm lab})] , \tag{54}$$

$$S_t = \tfrac{1}{4}[1 - D_{nn} + (D_{l'l} - D_{s's})/\cos(\theta_{\rm lab})] , \tag{55}$$

then the $L\cdot S$ distortions for $D_{l'l}$ and $D_{s's}$ will almost cancel. We also note that the distortions (or M^* effects) do not change the relation among the D_{ij} (which is always satisfied).

$$D_{s'l} + D_{l's} = (D_{l'l} - D_{s's})\tan(\theta_{\rm lab}) . \tag{56}$$

These spin-orbit distortion formulas Eqs. (40)—(46) are valid to order $R\langle N\rangle$. If the average $\langle N\rangle$ is very small (as it is at very forward scattering angles) then there will be terms of order $R^2\langle N^2\rangle$ (which is about $R^2/2$) which could be important.

V. RESULTS

In this section we summarize the results of Secs. III and IV for the spin observables in quasielastic scattering. In Table IV (see also Table V) we consider 500 MeV proton scattering from Pb at 18.5 deg. The polarization P is seen to decrease by 40% from the free value of 0.41 down to 0.25 (see Fig. 3). The vast majority of this reduction is due to the change in M^* rather than the $L\cdot S$ distortions (although they go in the same direction). The parameters $D_{s's}$, $D_{l'l}$ increase by 30% as M^* decreases but then the $L\cdot S$ distortions act in the opposite direction to cancel some of this increase. In fact, the measured $D_{s's}$ and $D_{l'l}$ (Ref. 15) are close to the free values. This null result could be understood if our estimate of the $L\cdot S$ distortions are somewhat too small. Finally, D_{nn} is not sensitive to either M^* or $L\cdot S$ effects.

The parameters $D_{s'l}$ and $D_{l's}$ are both increased in ab-

TABLE VI. Spin observables (average of pp and pn) at 800 MeV without $L\cdot S$ distortions.

$\theta_{\rm c.m.}$	$\theta_{\rm lab}$	P	D_{nn}	$D_{s's}$	$D_{s'l}$	$D_{l's}$	$D_{l'l}$
			$M^*=M$				
10°	4.2°	0.18	0.92	0.78	0.07	−0.07	0.83
30°	12.6°	0.42	0.90	0.77	0.30	−0.31	0.70
50°	21.3°	0.37	0.87	0.69	0.41	−0.45	0.60
			$M^*=0.89M$				
10°	4.2°	0.15	0.94	0.83	0.10	−0.10	0.87
30°	12.6°	0.33	0.90	0.82	0.32	−0.34	0.74
50°	21.3°	0.30	0.86	0.73	0.41	−0.44	0.63

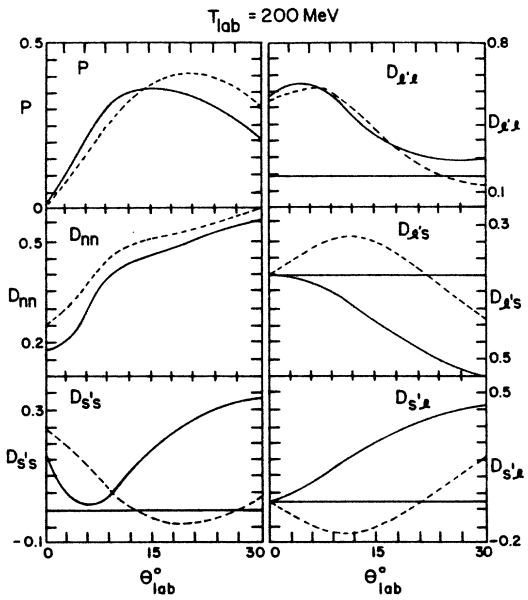

FIG. 5. Spin observables (average of pp and pn) at 200 MeV without $L\cdot S$ distortions versus laboratory scattering angle. The free $M^*=M$ results are dotted while the solid curves are for an M^* of $0.81M$.

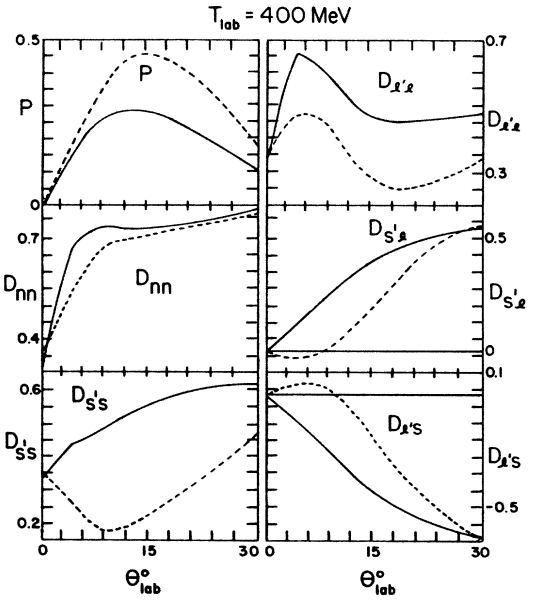

FIG. 6. Spin observable (average of pp and pn) at 400 MeV without $L\cdot S$ distortion versus laboratory scattering angle. The free $M^*=M$ results are dotted while the solid curves are for an M^* of $0.81M$.

solute value as M^* decreases. In addition, the $L\cdot S$ distortions act to further increase their magnitudes (in contrast to $D_{l'l}$, $D_{s's}$). Therefore, these parameters should be noticeably above the free values.

At 800 MeV (Table VI) the M^* effects are somewhat smaller with P decreasing by about 20%. The analyzing power has been measured in ^{181}Ta at 19.3 deg to be 0.29.[16] This is in good agreement with the predicted M^* effect where the free value of 0.37 is reduced to 0.30. Figure 4 shows the analyzing power in ^{12}C which agrees well with the reduced M^* value. The change in the other spin observables is less than 10%.

At low energies, 200 MeV (Table VII and Fig. 5), the polarization does not change much with M^*. However, the D_{ij} are very sensitive to M^*. With decreasing M^*, $D_{s'l}$ is much more positive (and $D_{l's}$ more negative). (At this low energy one should also consider corrections to the simple reaction mechanism from exchange and Pauli blocking.)

At 400 MeV (Table VIII and Fig. 6) the polarization is reduced by 40% as M^* decreases while D_{nn} is almost unchanged. Both $D_{s's}$ and $D_{l'l}$ are significantly enhanced while $D_{l's}$ and $D_{s'l}$ are also changed at forward angles.

It remains to evaluate corrections from multiple hard scattering (where two nucleons are ejected). Double scattering in light nuclei at the top of the quasielastic peak may be down by a factor of 10.[17] However, in heavy nuclei, multiple scattering is believed to substantially broaden the quasielastic peak at large angles. Even a crude estimate of the effects of multiple scattering on spin observables in heavy nuclei would be very useful.

VI. CONCLUSIONS

In this paper, we have considered the spin observables in quasielastic proton scattering. Given the success of many relativistic descriptions of elastic spin observables one should also examine inelastic scattering with its much

TABLE VII. Spin observables (average of pp and pn) at 200 MeV without $L\cdot S$ distortions.

$\theta_{c.m.}$	θ_{lab}	P	D_{nn}	$D_{s's}$	$D_{s'l}$	$D_{l's}$	$D_{l'l}$
				$M^*=M$			
10°	4.8°	0.13	0.34	0.17	−0.09	0.12	0.51
30°	14.3°	0.37	0.51	−0.02	−0.13	0.22	0.32
50°	23.9°	0.40	0.56	−0.02	0.06	−0.05	0.00
				$M^*=0.81M$			
10°	4.8°	0.17	0.24	0.02	0.07	−0.02	0.56
30°	14.3°	0.37	0.46	0.17	0.27	−0.25	0.28
50°	23.9°	0.31	0.53	0.30	0.41	−0.50	0.09

TABLE VIII. Spin observables (average of pp and pn) at 400 MeV without $L\cdot S$ distortions.

$\theta_{c.m.}$	θ_{lab}	P	D_{nn}	$D_{s's}$	$D_{s'l}$	$D_{l's}$	$D_{l'l}$
				$M^*=M$			
10°	4.5°	0.21	0.56	0.26	−0.03	0.05	0.48
30°	13.7°	0.46	0.71	0.21	0.16	−0.13	0.30
50°	23.0°	0.35	0.75	0.35	0.46	−0.48	0.27
				$M^*=0.81M$			
10°	4.5°	0.17	0.69	0.44	0.13	−0.12	0.66
30°	13.7°	0.29	0.73	0.55	0.38	−0.40	0.48
50°	23.0°	0.20	0.76	0.61	0.51	−0.57	0.46

richer choice of spin observables. Furthermore, quasielastic scattering to the continuum may minimize one's sensitivity to the unknown nuclear structure of the excited states.

The lower components of a nucleon's wave function may be substantially enhanced in the strong nuclear potential. Furthermore, successful RIA descriptions of elastic scattering make definite and easily calculated assumptions about how the NN interaction will change with the enhanced lower components. We find that due to this M^* effect the polarization is decreased by almost 40% at 500 MeV. We emphasize that spin observables may allow one to test the assumed relativistic form of the NN interaction.

For these calculations we have used an eikonal model which yields an average effective mass M^* of 0.8 to $0.9M$. This value is higher than the MFT value of $0.56M$ because the reaction is surface peaked. However, the NN interaction was found to be sensitive to even small changes in M^* because of strong cancellations between very large Lorentz components.

We have also provided simple estimates of how distortions from the spin-orbit optical potential change spin observables. At 500 MeV and 18.5 deg in Pb the polarization is decreased by less than 5% while $D_{l'l}$ and $D_{s's}$ are decreased by 15%. The simple formula, Eqs. (40)—(46), may be useful in other nonrelativistic models.

Much remains to be done. First, more measurements of quasielastic spin observables would help. One should measure the D_{ij} at both higher (800 MeV) and lower (200, 400 MeV) energies than the existing 500 MeV LAMPF data. Note, even if it is not possible to measure sideways (or longitudinal) polarization, an incomplete set of D_{ij} would still be useful. Data for a range of A might allow one to separate M^* effects (which may be approximately constant with A) from multiple scattering corrections which should grow with A.

Second, one should try and estimate the effects of multiple scattering on spin observables in heavy nuclei. In addition, it is important to examine other forms for the relativistic NN interaction besides the simple local Eq. (2). For example, one can replace the pseudoscalar γ_5 in Eq. (2b) with a pseudovector $\not{q}\gamma_5$ term or use the more complicated interaction in Ref. 18. The quasielastic data should then provide useful constraints on the relativistic form of the NN interaction.

ACKNOWLEDGMENTS

C.H. thanks the theory group at TRIUMF for the very kind hospitality. Useful discussions were had with E. Cooper, J. Shepard, T. Drake, A. Miller, K. Hicks, O. Hausser, and J. Moss. This work was supported in part by funds provided by the U.S. Department of Energy (D.O.E.) under Contract No. DE-AC02-76ER03069.

APPENDIX A

Here we give the relation between $a,\ldots,e$ and Lorentz invariants $F_s,\ldots,F_v$ in Eq. (17). The matrix $[M]$ is written as a product of two matrices

$$[M]=ik_c[A][B]\ . \tag{A1}$$

The matrix $[A]$ is given in Table IX while $[B]$ is listed in Table X using the symbols defined in Table XI. The momentum k_c and scattering angle θ are in the center of mass frame.

TABLE IX. The matrix $[A]$ in Eq. (A1).

A	1	2	3	4	5
a	$\cos\theta$	$\cos\theta$	$\cos\theta$	$-\cos\theta$	$-4\sin\theta$
b	1	−1	1	1	0
c	−1	1	1	1	0
d	1	1	−1	1	0
e	$-i\sin\theta$	$-i\sin\theta$	$-i\sin\theta$	$i\sin\theta$	$-4i\cos\theta$

TABLE X. The matrix $[B]$ in Eq. (A1). The matrix elements are listed in Table XI.

B	F_s	F_v	F_p	F_a	F_t
1	α	$e\alpha+p\beta$	0	$p\alpha+e\beta$	-2β
2	$-e\gamma$	$-\gamma$	$-p\gamma$	$-\delta$	$2(p+e)\delta$
3	α	$(p+e)\alpha$	0	$(-p+e)\alpha$	2α
4	$e\gamma$	γ	$-p\gamma$	$-\gamma$	2γ
5	$-\epsilon$	$-\epsilon$	0	ϵ	-2ϵ

TABLE XI. Matrix elements for Table X.

$\alpha=$	$\cos^2\theta/2$
$\beta=$	$1+\sin^2\theta/2$
$\gamma=$	$\sin^2\theta/2$
$\delta=$	$1+\cos^2\theta/2$
$\epsilon=$	$E_c^*/M^*\sin\theta/2\cos\theta/2$
$E_c^*=$	$(k_c^2+M^{*2})^{1/2}$
$e=$	E_c^{*2}/M^{*2}
$p=$	k_c^2/M^{*2}

APPENDIX B

In this appendix we give the expressions for different polarization transfer observables in the terms of a, b, c, d, and e amplitudes. These expressions are given in Ref. 11. We collect them here for completeness. Consider nucleon-nucleon scattering. Let θ be the scattering angle in the two-body center-of-mass and $\theta_{\rm lab}$ the angle in the laboratory system. Define

$$\alpha=\frac{\theta}{2}-\theta_{\rm lab}\ . \tag{B1}$$

Then the various polarization transfer observables and the corresponding Wolfenstein parameters are given by the following formulas.

$$D=D_{nn}=(\,|a|^2+|b|^2-|c|^2-|d|^2+|e|^2)/\sigma\ ,$$

$$R=D_{s's}=A\sin(\alpha)\sin\left[\frac{\theta}{2}\right]-B\sin\left[\alpha+\frac{\theta}{2}\right]+C\cos(\alpha)\cos\left[\frac{\theta}{2}\right]\ ,$$

$$A=D_{s'l}=-A\sin(\alpha)\cos\left[\frac{\theta}{2}\right]-B\cos\left[\alpha+\frac{\theta}{2}\right]-C\cos(\alpha)\sin\left[\frac{\theta}{2}\right]\ , \tag{B2}$$

$$R'=D_{l's}=A\cos(\alpha)\sin\left[\frac{\theta}{2}\right]+B\cos\left[\alpha+\frac{\theta}{2}\right]+C\sin(\alpha)\cos\left[\frac{\theta}{2}\right]\ ,$$

$$A'=D_{l'l}=A\cos(\alpha)\cos\left[\frac{\theta}{2}\right]-B\sin\left[\alpha+\frac{\theta}{2}\right]-C\sin(\alpha)\sin\left[\frac{\theta}{2}\right]\ .$$

Here

$$\sigma=\tfrac{1}{2}(\,|a|^2+|b|^2+|c|^2+|d|^2+|e|^2) \tag{B3}$$

and

$$\begin{aligned} A&=\mathrm{Re}(a^*b-c^*d)/\sigma\ ,\\ B&=\mathrm{Im}(b^*e)/\sigma\ ,\\ C&=\mathrm{Re}(a^*b+c^*d)/\sigma\ . \end{aligned} \tag{B4}$$

The corresponding nonrelativistic formulas can be obtained by putting $\alpha=0$ in the above relations. The subscripts n, l, and s on the D observables denote the components along the normal, longitudinal (direction of the beam), and the sideways directions [see Fig. 2(a)].

[1] C. J. Horowitz and Brian D. Serot, Nucl. Phys. **A368**, 503 (1981).

[2] L. G. Arnold *et al.*, Phys. Rev. C **23**, 1949 (1981); B. C. Clark *et al.*, *The Interaction Between Medium Energy Nucleons in Nuclei—1982,* Proceedings of the Workshop on the Interaction Between Medium Energy Nucleons in Nuclei, AIP Conf. Proc. No. 97, edited by H. O. Meyer (AIP, New York, 1983).

[3] J. A. McNeil, J. Shepard, and S. J. Wallace, Phys. Rev. Lett. **50**, 1439 (1983); J. Shepard, J. A. McNeil, and S. J. Wallace, *ibid.* **50**, 1443 (1983).

[4] C. J. Horowitz, Phys. Rev. C **31**, 1340 (1985).

[5] R. Amado *et al.*, Phys. Rev. C **28**, 1663 (1983).

[6] J. D. Walecka, Ann. Phys. (N.Y.) **83**, 491 (1974).

[7] A. M. Kabos, E. D. Cooper, J. I. Johansson, and H. S. Serif, Nucl. Phys. **A445**, 605 (1985).

[8] D. M. Corely *et al.*, Nucl. Phys. **A184**, 437 (1972).

[9] F. R. Kroll and N. S. Wall, Phys. Rev. C **1**, 138 (1970).

[10] R. Rosenfelder, Ann. Phys. (N.Y.) **128**, 188 (1980).

[11] J. Brstricky, F. Lehar, and P. Winternitz, J. Phys. (Paris) **39**, 1 (1978).

[12] J. A. McNeil, L. Ray, and S. J. Wallace, Phys. Rev. C **27**, 2123 (1983).

[13] R. A. Arndt and D. Roper, VPI and SU Scattering Analysis Interactive Dialin Program and Data Base.

[14] L. S. Celenza, W. S. Pong, and C. M. Shakin, Phys. Rev. C **25**, 3115 (1982); C. J. Horowitz and B. D. Serot, Phys. Lett. **137B**, 287 (1984).

[15] T. A. Carey *et al.*, Phys. Rev. Lett. **53**, 144 (1984).

[16] S. Frankel *et al.*, Phys. Rev. Lett. **41**, 148 (1978).

[17] R. D. Smith and S. J. Wallace, Phys. Rev. C **32**, 1654 (1985).

[18] J. A. Tjon and S. J. Wallace, Phys. Rev. C **32**, 667 (1985).

[19] J. A. McGill *et al.*, Phys. Lett. **134B**, 157 (1984).

[20] G. Do Dang and Nguyen Van Giai, Phys. Rev. C **30**, 731 (1984).

[21] A. Picklesimer, J. W. Van Orden, and S. J. Wallace, Phys. Rev. C **32**, 1312 (1985).